Space quantum communication networks

Duncan McArthur[a], Jasminder Sidhu[a], Colin Aitken[b], Owain Pryce-Jones[c], Mark Bowyer[d], Markus Krutzik[f,e], Mustafa Gündoğan[e], and Daniel K. L. Oi[a]

[a]SUPA Department of Physics, University of Strathclyde, Glasgow G4 0NG, United Kingdom
[b]Craft Prospect Limited, Glasgow, G51 4XS, United Kingdom
[c]Archangel Lightworks Limited, London, SE1 3XF, United Kingdom
[d]Airbus Defence and Space Limited, Stevenage, SG1 2AS, United Kingdom
[e]Institut für Physik and IRIS Adlershof Humboldt-Universität zu Berlin, Newtonstr. 15, Berlin 12489, Germany
[f]Ferdinand-Braun-Institut (FBH), Gustav-Kirchoff-Str. 4, Berlin 12489, Germany

ABSTRACT

Satellite constellations have the potential for enabling globe-spanning quantum networks for secure communication, entanglement distribution, and eventually the quantum internet. The architecture, design, and operation of such space quantum networks face several challenges, from scheduling, performance analysis and optimization, and overcoming issues such as weather effects. Here, we summarise recent research into constellation design, optimization, and the incorporation of quantum memories and repeaters in space quantum communication links. These preliminary works offer guidance for future development efforts for long-term space quantum communication systems.

Keywords: quantum-key-distribution (QKD), quantum networks, cryptography, satellite communication

1. INTRODUCTION

Space-based quantum communication networks will help unlock the potential of quantum technologies.[1] An ideal quantum network enable high-rate communications over long-ranges. In practice, signal losses pose a challenge in achieving both high-rate communications and long-range networks. In this work, we analyse and review two applications of space networks to enable global quantum communication coverage. First, we look at a trusted-node quantum key distribution (QKD) system for secure communications between an airborne segment and a satellite constellation. As part of a system architecture study, we explore the finite-key performance of a single satellite-based downlink employing the weak-coherent pulse decoy-state Bennett Brassard 1984 (BB84) protocol and quantify the impact of the satellite's altitude on the key generation footprint, an important input into constellation sizing. Second, we cover candidate space quantum communication network architectures that could support both high-rate and long-range entanglement distribution utilising space quantum memories. With entanglement distribution crucial for the development of global networked quantum computers, sensors, positioning, navigation and timing, as well as for fundamental tests of physics,[2] these architectures may reveal outstanding technical and scientific obstacles, and provide guidance for future development.

2. SATELLITE CONSTELLATION FOR AIRBORNE SEGMENT QKD

To support global quantum secure communications, trusted-node satellite QKD will be initially deployed, with efforts in China,[3] Europe,[4] and Canada,[5] for example. Research has mainly concentrated upon enabling secure communications between terrestrial nodes and networks.[6–10] In this section, we present preliminary analysis of a satellite constellation design to provide secure connectivity to the air segment, nominally commercial airliners at cruising altitude above the majority of weather interruptions and atmospheric attenuation. The QKD constellation can also provide secure links to other satellites if they are fitted with suitable QKD transmitters. In this section, we focus upon the task of determining the optimum orbital altitude for maximising the QKD generation footprint of each satellite, hence reducing the number of satellites required for global coverage.

Further author information: Corresponding author DKLO
E-mail: daniel.oi@strath.ac.uk, Telephone: +44 (0)141 548 3112

Quantum Computing, Communication, and Simulation V, edited by Philip R. Hemmer, Alan L. Migdall, Proc. of SPIE Vol. 13391, 1339102 · © 2025
SPIE · 0277-786X · doi: 10.1117/12.3040186

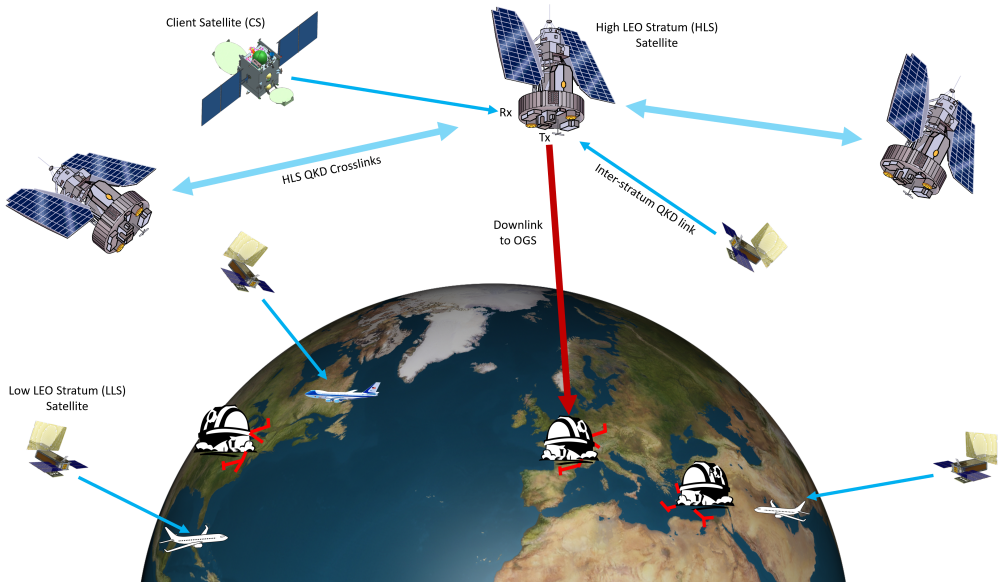

Figure 1. **QKD Constellation Concept Architecture.** The constellation consists of a low LEO stratum (LLS) and high LEO stratum (HLS). The numerous LLS satellites, equipped with transmitters (Tx) are small/relatively inexpensive and provide connectivity to airliners equipped with receivers (Rx). The LLS satellites are deployed across several orbital planes to maximise coverage of the airborne segment and ensure that an aircraft will have a QKD downlink opportunity during its cruising phase. The QKD keys generated by the LLS satellites with the aircraft and then relayed to the HLS satellites for onward distribution, either to other aircraft, the space segment, or downlink to a terrestrial network. The HLS consists of a single orbital plane (sun synchronous or polar orbit) with several larger HLS satellites equipped with Rx apertures to link with the LLS and client satellites. They also have intersatellite QKD crosslinks between themselves to relay keys across the HLS. The HLS satellites also possess downlink-optimised transmitters to establish keys with optical ground stations (OGSs) and their local networks. The optical links between the LLS and aircraft, and between satellites are vacuum optimised in order to reduce aperture size required to achieve acceptable channel diffraction losses. We note that dual-layer QKD constellation has been proposed in Ref.[11] for connecting terrestrial networks.

Fig. 1 illustrates the overall system concept. It consists of a dual strata configuration in low Earth orbit (LEO). The lower LEO stratum (LLS) consists of smallsats (nominally CubeSats or microsats) with QKD transmitters that can establish secure keys with aircraft below or satellites in the upper layer. The upper layer, called the high LEO stratum (HLS) receives QKD signals from the LLS as well as client satellites that require QKD services. The HLS satellites have inter-satellite QKD links to allow for key relay across this layer as well as downlink transmitters to establish QKD keys with the terrestrial segment. For the purposes of this paper, we do not consider this latter aspect of the architecture as this is already well-studied (Ref.[12] for example). We will however concentrate on the analysis of the LLS and the space-air link.

2.1 Space-Air Link Scenario

We consider the link between a satellite transmitter and a receiver mounted on an aircraft assumed to be at a cruising altitude of 10 km. This largely removes the need to consider cloud penetration in modeling the system as this is typically above the dense cloud strata, hence we assume clear sky conditions. Atmospheric absorption and scattering is also reduced compared with sea-level receivers, resulting in lower channel losses and background light, even during daytime conditions. The overpass geometry is shown in Fig. 2. Our estimate of the channel transmission versus loss for different wavelengths is shown in Fig. 3 for a baseline satellite altitude of 500 km (the loss curve was recalculated for each altitude) [*]. To simplify the calculations we take the aircraft to be stationary with respect to the satellite due to the high orbital speed ($\sim$ 7.5 km/s) versus the aircraft ($\sim$ 300 m/s). We consider satellites in a range of LEO with the satellite altitude $h_{\rm sat} \leq 2000$ km.

[*]The effect of boundary layer turbulence has been studied by other workers, see Refs[13–15] for example. The results of Ref.[15] are not directly comparable with our scenario as they assume a different wavelength, receiver diameter, and single-mode coupling without higher-order adaptive optics.

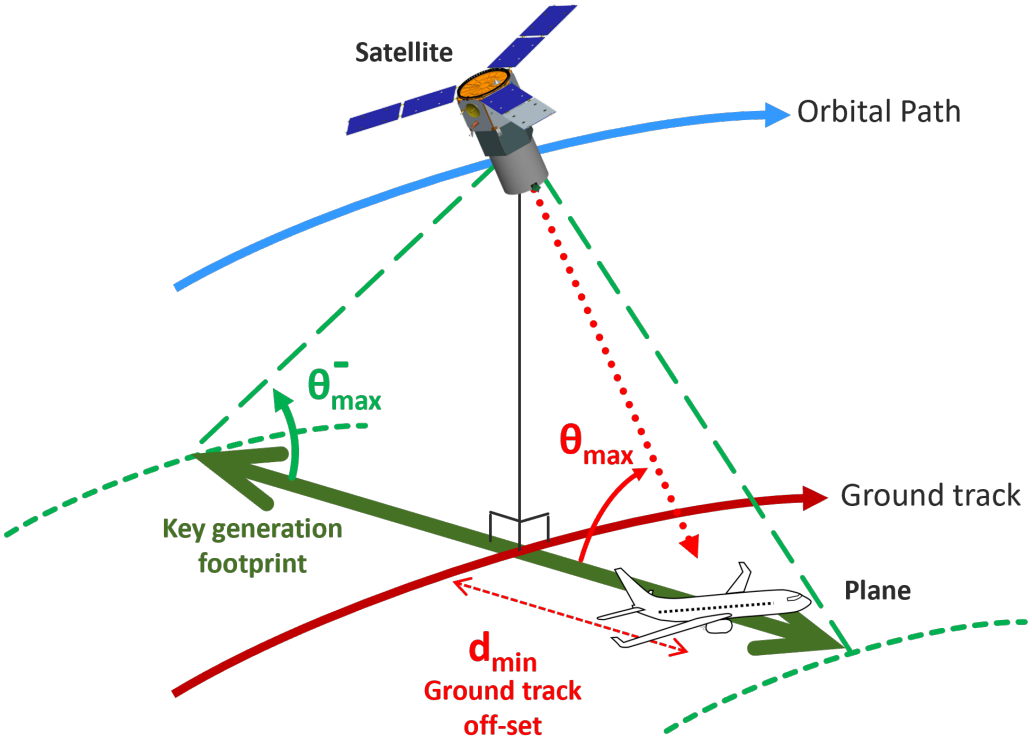

Figure 2. **Overpass Geometry**. We assume that the aircraft is relatively stationary compared with the orbital velocity of the satellite. The closest approach of the ground track to the aircraft is d_{min}. The smallest θ_{max} which results in the required amount of SKL is denoted θ^{-}_{max} and the key generation footprint is given by $2d_{min}$ for this case. We do not impose any field of regard limits on the airborne receiver in this study, though this should be considered in a more comprehensive analysis.

Based on the trends in Fig. 3, we focus on UV wavelengths for transmission links as it provides reduced diffraction losses, allows for smaller receiver apertures, and is associated to lower background light levels compared to typical near-infrared transmission wavelengths. Additionally, we choose 397 nm as this coincides with a Fraunhofer line in the solar spectrum that further reduces background light levels.[18]

For the estimate of the secret key length (SKL), we employ the efficient BB84 protocol in a downlink configuration, applying a finite block treatment, where all of the free parameters are optimized (see Refs[9,10]). We use the modeling software suite SatQuMA for all calculations[19] and the full set of system parameters is listed in Table 1.

2.2 Key Generation Footprint Results

Figure. 4 shows the single-pass finite-block SKL generated for a range of satellite altitudes, $h_{\rm sat}$, as a function of two variables. The first variable (shown in the left column) is the maximum elevation of the overpass, $\theta_{\rm max}$, of the satellite with respect to the aircraft receiver. The second variable (right column) is the key generation footprint (KGF) of the satellite orbit with respect to the aircraft receiver, which is related to the lateral offset of the satellite ground track to the aircraft (the KGF is twice the offset, taking into account the symmetry of the overpasses on either side of the aircraft). The KGF defines the width of swath under the satellite for which an aircraft can obtain the required amount of secure key during a single overpass.[9] We investigate the SKL generated as a function of these two variables for transmission windows of $\Delta T = \{60, 300\}$ s, with the short and long durations in the top and bottom row, respectively. The SKL data is the same for both variables (left and right columns of Fig. 4), however when we increase the transmission duration, we see an overall increase of the SKL by a factor of ~ 3 while the absolute maximum SKL observed increases by a factor of ~ 2.

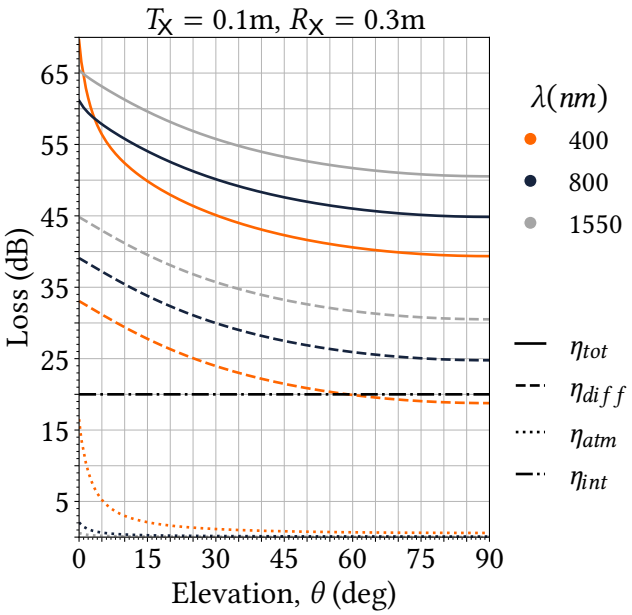

Figure 3. **Channel loss between an LLS Satellite and Aircraft**. We show a representative loss vs elevation graph for a satellite in a 500 km altitude orbit transmitting photons to an aircraft cruising at 10 km altitude. The total loss η_{tot} is modeled as a combination of the diffraction loss η_{diff}, atmospheric losses η_{atm}, and a loss component η_{int} intrinsic to the system (internal receiver losses, detector inefficiency, coupling losses). A conservative value of $\eta_{int} = 20$ dB is estimated from an optimised fit to Micius data (see Ref.[9]) and also includes upper bounds to unresolved losses due to pointing and turbulence. Here we show these loss components as a function of elevation for three transmission wavelengths, where receiver and transmitter diameters are $R_X = 300$ mm and $T_X = 100$ mm respectively. The atmospheric transmissivity was determined using MODTRAN.[16] Typically considered wavelengths for satellite QKD are either C-Band ~ 1550 nm due to telecoms heritage, or near infrared (NIR) ~ 800 nm due to the availability of silicon single-photon avalanche detectors sensitive in this spectral region. Shorter wavelengths are usually not considered due to high atmospheric scattering and absorption for terrestrial up/downlink, but for high altitude and vacuum links such losses are greatly reduced or eliminated.[17] The lower diffraction enables the use of smaller apertures, leading to system size and weight reduction.

The maximum elevation data shows some expected trends: lower altitude orbits can generate more SKL and maintain a link at lower elevations, while orbits closer to zenith (above the receiver) always generate the most SKL. This is due to the reduced path between transmitter and receiver for a lower orbit, hence lower losses. As we increase the transmission window duration, the critical maximum elevation $\theta^{-}_{\max}$ (see Fig. 2) for each orbital altitude decreases, indicating that the link is providing greater amounts of key at lower elevations.

For the KGF data, the trends are slightly more complex. For a receiver close to the satellite ground track (zenith), the ordering of the results is the same as before. However, as the receiver moves laterally away from the ground track we see some of the higher altitude curves cross those of the lower altitudes. This trend increases as we reduce the total loss in the system (not shown) and the highest altitude LEO orbits perform best in terms of KGF under those conditions.

For the short transmission window $\Delta T = 60$ s, the maximum KGF (where non-zero SKL is achieved) is found for an orbital altitude of $h_{\text{sat}} = 530$ km. While for $\Delta T = 300$ s, the maximum KGF is found for $h_{\text{sat}} = 560$ km. These results show that higher altitude satellite orbits typically provide greater 'ground' coverage, potentially reducing the number of satellites required for a communications network. If a minimum SKL per overpass is needed (we take the values of 100 and 1000 AES-256 keys for short and long haul flight respectively), this restricts the allowable KGF to a smaller value. This results in an optimum LLS altitude of ~ 560 km resulting in a KGF of > 2000 km. In order to guarantee that a short haul flight, with a minimum cruise altitude time of 10 mins, is able to receive 100 AES-256 keys, the LLS may consist of 10 polar orbit planes with 10 satellites in each orbital plane, assuming day and night time operation of the QKD link.

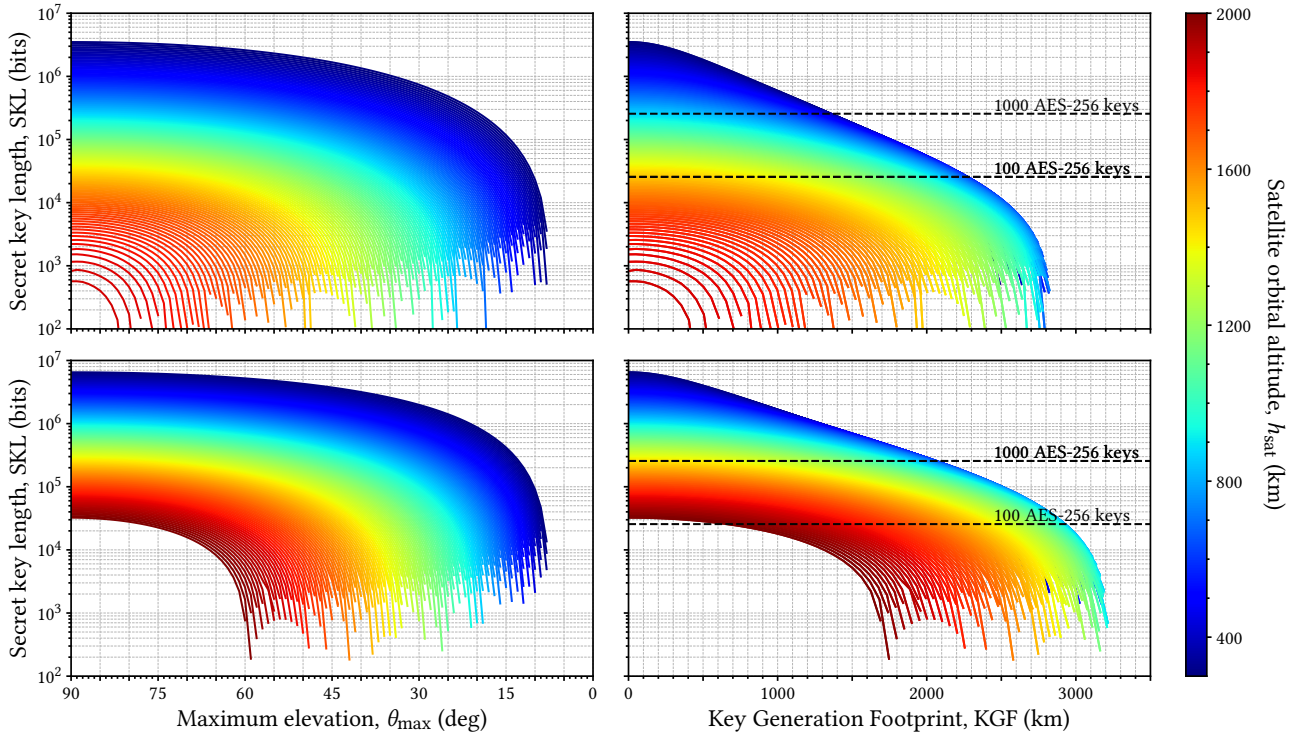

Figure 4. **Secret key length vs maximum elevation angle and key generation footprint**, each for different satellite altitudes. Results shown for a short transmission window of 60 s (top row) and a longer transmission window of 300 s (bottom row). These times are assumed to be minimum available periods at cruise altitudes for short and long haul flights respectively. All other parameters are the same and are listed in Table 1.

Parameter description	**Notation**	**Value**
Transmitter aperture diameter	T_X	10 cm
Receiver aperture diameter	R_X	30 cm
Gaussian beam waist	w_0	5 cm
Source wavelength	λ	397 nm
Source rate	f_s	1 GHz
Airplane cruising altitude	h_{air}	10 km
Intrinsic quantum bit error rate	$QBER_I$	0.1%
Extraneous count probability	p_{ec}	10^{-7}
After-pulsing probability	p_{ap}	0.1%
System loss metric	η_{loss}^{sys}	40 dB
Correctness parameter	ϵ_c	10^{-15}
Security parameter	ϵ_s	10^{-10}

Table 1. **Reference system parameters.** Transmitter, receiver, and source properties determine range and elevation-dependent loss. The system loss metric, η_{loss}^{sys}, defined as the link efficiency at zenith, is 40 dB for a nominal 500 km orbital altidue. η_{loss}^{sys} can be scaled to model other SatQKD systems that differ by a fixed link loss ratio, e.g. different T_X or R_X apertures, or detector efficiencies. The intrinsic quantum bit error rate, $QBER_I$, incorporates errors from source quality, receiver measurement fidelity, basis misalignment, and polarization fluctuations, while the extraneous count probability, p_{ec}, incorporates detector dark count and background rate. The correctness and security parameters are used to determine the finite-block composable SKL.

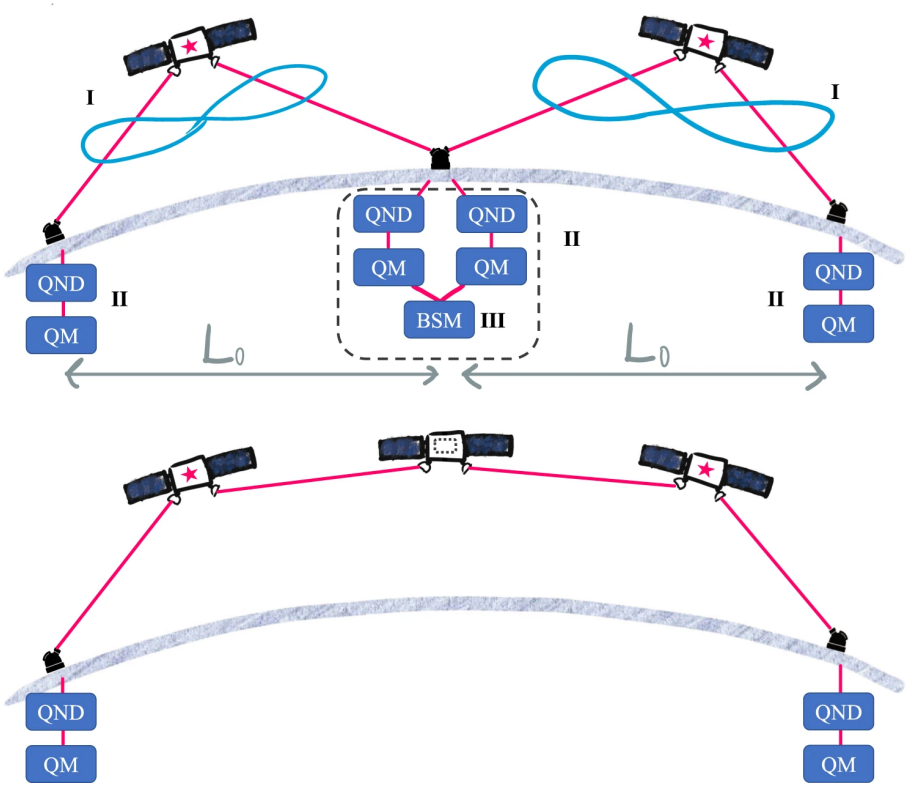

Figure 5. **Satellite Quantum Repeaters**. Figure reproduced from Ref.[25] (Top) An initial proposal[26] utilised a hybrid scheme where satellites distributed entangled pairs to ground stations (I). Intermediate terrestrial repeater nodes equipped with quantum memories (II) would perform entanglement swapping (III). (Bottom) Alternatively, quantum repeater nodes an be placed on satellites co-orbiting with the entanglement sources.[25] This reduces losses due to multiple atmospheric passes as well as reduced challenges associated with intermediate node placement geography, weather outage, and overpass geometry. The trade-off is that quantum memories would need to be placed in orbit.

3. SPACE QUANTUM MEMORIES FOR ENTANGLEMENT DISTRIBUTION

Beyond key distribution, quantum communication networks will enable distributed quantum technologies. Global-scale quantum networking faces significant technical and scientific obstacles. Direct transmission of quantum signal through optical fibres is limited by inherent exponential losses. Alternatively, satellite links can establish lower loss channels. The Micius satellite demonstrated direct distribution of entangled pairs to OGSs more than 1000 km apart, though at rates ~ 1 pair/s,[20] with this dual downlink configuration studied in Refs[21–24] for example. Quantum repeaters (QRs) have been proposed as a solution to overcome the limits of direct transmission. However, terrestrial fibre-based QRs are typically limited to a total distance of a few thousand kilometers and/or require extensive hardware overhead. In this section, we very briefly highlight recent satellite quantum-memory and quantum-repeater-based proposals that enable entanglement distribution over global scales.

3.1 Space-borne Quantum Repeaters

The first study on satellite architectures for entanglement distribution proposed a hybrid space-ground quantum repeater (QR) system,[26] where quantum memories (QMs) were situated at ground stations. However, this approach suffered from low transmission rates over large distances, particularly at low satellite elevation angles. To address this, subsequent works proposed fully satellite-based QRs,[25,27] leveraging advancements in atomic physics[28] (Fig. 5). In these architectures, QMs are located onboard satellites, thereby reducing the number atmospheric quantum links. These studies demonstrated the feasibility of global entanglement distribution using a satellite network equipped with QMs and entangled photon sources (Fig. 6). Specifically, storage times of $\sim$1s is sufficient to enable global distribution,[25,27] while intercontinental links exceeding 8000 km is possible with memory lifetimes of around 100 ms.[25,29]

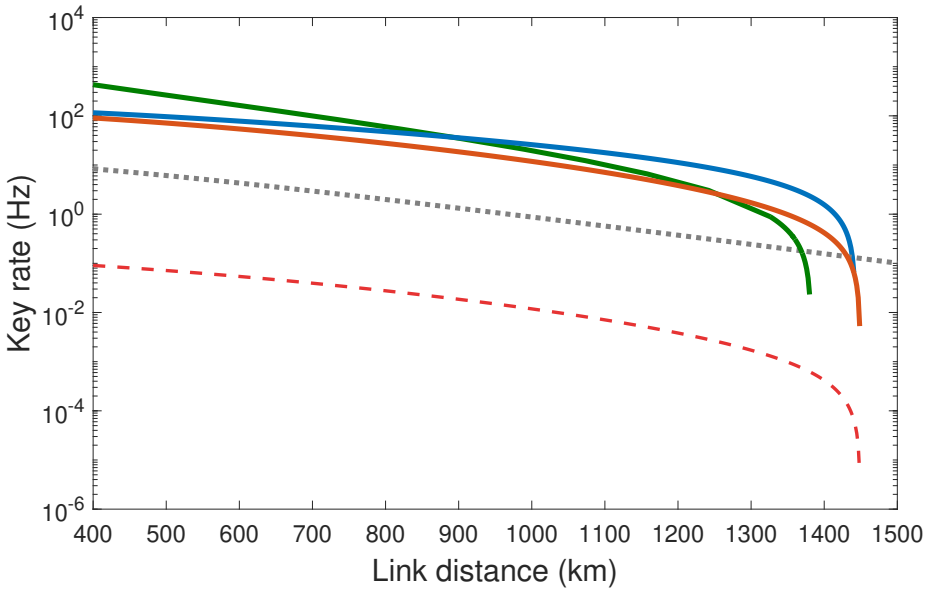

Figure 6. **Single satellite quantum repeater QKD performance**. Figure reproduced from Ref.[25] Grey dotted: Direct dual down link ent-QKD (source rate $R_s = 20$ MHz); blue: dual uplink configuration with storage time 5 ms; solid (dotted) red: quantum memory assisted downlink configuration, with N=1000 (single) temporal modes with storage time 7.5 s; green: downlink with N = 1000 temporal modes and m=100 memory pairs with storage time 100 ms.

3.2 Space Quantum Courier

An alternative to QR constellations[25] is to take advantage of a single satellite equipped with a single long-lived quantum memory, with the trade-off advantage of reduced system complexity and coordination of simultaneous optical links. Intuitively, long-lived quantum memories (∼hr) allow the physical transportation of stored qubits to improve entanglement distribution rates, and were first proposed in 2017.[30] A recent proposal used a second shorter-lived quantum memory (∼ms) to effectively serve as a time-delayed version of a single QR node[31] (Fig. 7 Left). The inclusion of a second, shorter-lived quantum memory improves long-distance entanglement distribution.

Using QKD as a benchmark for entanglement distribution, the amount of secure key in the finite block regime was improved by three orders of magnitude over the use of a single quantum memory (Fig. 7 Right). The main effect of the second QM is to greatly increase the number of distributed raw pairs between OGSs A and B at the slight cost of reduced entanglement fidelity. The improvement in number of pairs scales with the single channel loss as all the stored entanglement can be downlinked. The greater block size has the 2-fold effect of increasing the number of pairs from which to distill a secure key and reducing the finite statistical uncertainties in the parameter estimation that can significantly impact small block sizes.

4. DISCUSSION AND CONCLUSIONS

In the near term, the use of trusted-node QKD satellite networks may provide practical security for certain applications and threat scenarios. Extending secure communications to all segments of the global communication network will be important to ensure consistent security between different end-nodes, including aircraft. Commercial airlines are a potential use-case, not only for passenger services but also for aircraft management and navigation (including autonomous guidance), especially taking into account increased automation and remote management of aircraft systems. Satellite optical communication systems are likely to be incorporated into airliners to cope with increased classical communication demands for in-flight services, hence provision of QKD capability should be considered. The analysis presented in Section 2 indicates that global in-flight QKD delivery to short and long haul airliners should be possible with a dual stratum constellation. The number of LLS satellites and orbital planes can be scaled to address the number and distribution of flights to be serviced

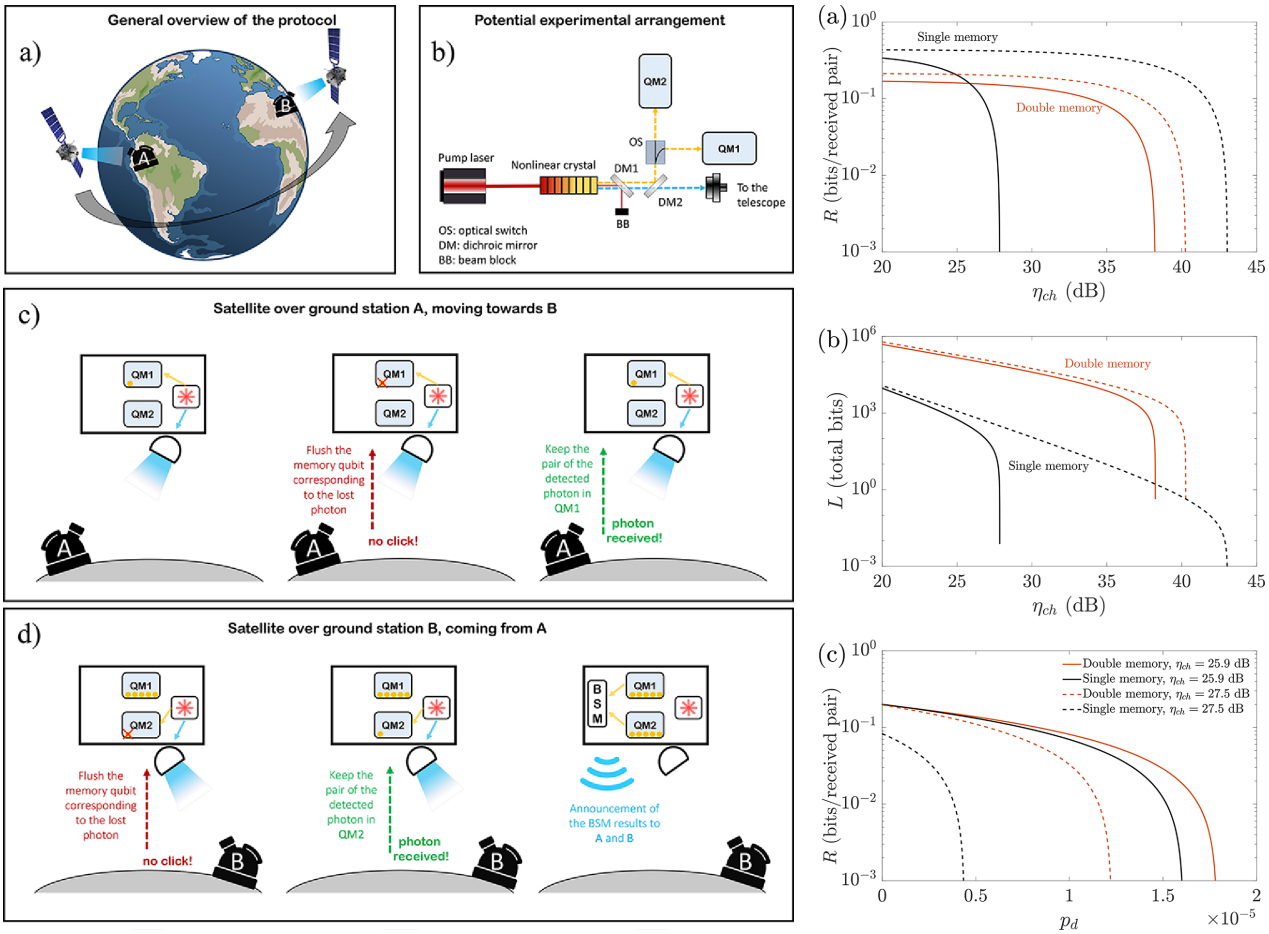

Figure 7. (Left) **Space Quantum Courier Concept**. Extending upon the proposal in Ref.,[30] single satellite carries two quantum memories instead of one. (a) General Overview of Scheme. Quantum memory QM1 serves as a long-duration storage of entanglement distributed on a first downlink to OGS A, sufficient for half the orbital period of the satellite. Quantum memory QM2 is used as part of the quantum repeater and entanglement swapping protocol on the second downlink to OGS B. (b) Proposed experimental setup depicting the entangled photon pair generation and absorptive memories. The photons in orange and blue modes are entangled. (c) One photon of the entangled pair is stored in the long-lived QM1, whereas its partner is sent to OGS A which heralds the satellite if it was received. If OGS A does not receive the photon, the respective QM1 mode is reset and ready for further entanglement distribution attempts, otherwise the stored photon is kept in QM1 for transport. This continues until all storage modes of QM1 are full or the transmission window is exceeded. (d) The satellite continues in its orbit and passes close to OGS B. We use QM2 in a similar process as for the OGS A overpass to establish shared entanglement with OGS B. Entanglement swapping is now performed by applying a Bell State Measurement to the stored photons in QM1 and QM2 whose result is broadcast to ground stations A and B who may perform local unitary corrections to distill a secret key or to restore their shared entangled pair. (Right) **Comparison of a single or dual memory equipped quantum courier satellite**. (a) Finite key rate per received pair (R) for (solid/dashed curves finite/asymptotic key rate); (b) total finite key length (L) as a function of average single channel loss (η_{ch}) for memory error rate $\epsilon = 5\%$ (solid/dashed curves finite/asymptotic key length). (c) Finite key rate per received pair versus total incoherent noise for fixed channel losses. Figures reproduced from Ref.[31]

concurrently. The QKD rates may be sufficient to secure communications for the aircraft systems and a modest number of passengers. The HLS layer can be optimised for terrestrial downlink as well as providing QKD services to client satellites. A more comprehensive account of the system architecture and its analysis, including intersatellite link budgets and HLS sub-system sizing, will be presented in future work.

In the longer term, applications beyond QKD will become important, requiring the long-distance distribution of quantum entanglement. The development of quantum memories for quantum repeaters is a significant challenge, though there have been promising advances in the duration and number of storage modes demonstrated (see the review Ref.[32]). Space operations introduces particular challenges such as size, weight, and power constraints, particularly if cryogenic systems are required, for example for some solid-state systems. In the longer term, when entanglement purification and error correction may need to be performed on the satellite, integrated quantum memory and processing systems will be required, indicating the development of specialised quantum computers with optical quantum interfaces. The use of optically interconnected ion-trap quantum computers[33,34] dedicated to error correction and entanglement purification is one possibility. This would allow scale-up of memory storage modes (e.g. through segment traps and shuttling), provide high fidelity quantum logic operations for purification, and not require cryogenic systems to operate.

ACKNOWLEDGMENTS

All authors acknowledge support from the EPSRC International Network in Space Quantum Technologies (EP/W027011/1). DKLO and DM acknowledge support from the Innovate UK project ViSatQT (Project number: 43037). DKLO and JS acknnowledge support from the EPSRC Quantum Technology Hub in Quantum Communication (EP/T001011/1).

REFERENCES

[1] Sidhu, J. S., Joshi, S. K., Gündoğan, M., Brougham, T., Lowndes, D., Mazzarella, L., Krutzik, M., Mohapatra, S., Dequal, D., Vallone, G., Villoresi, P., Ling, A., Jennewein, T., Mohageg, M., Rarity, J., Fuentes, I., Pirandola, S., and Oi, D. K. L., "Advances in space quantum communications," *IET Quant. Comm.* , 1–36 (2021).

[2] Belenchia, A., Carlesso, M., Bayraktar, Ö., Dequal, D., Derkach, I., Gasbarri, G., Herr, W., Li, Y. L., Rademacher, M., Sidhu, J., Oi, D. K., Seidel, S. T., Kaltenbaek, R., Marquardt, C., Ulbricht, H., Usenko, V. C., Wörner, L., Xuereb, A., Paternostro, M., and Bassi, A., "Quantum physics in space," *Physics Reports* **951**, 1–70 (2022). Quantum Physics in Space.

[3] Jones, A., "China is developing a quantum communications satellite network." https://spacenews.com/china-is-developing-a-quantum-communications-satellite-network/ (2024). Accessed: 2015-01-08.

[4] Antoni, N., Adriaensen, M., and Giannopapa, C., "Institutional space security programs in Europe," *Handbook of space security: policies, applications and programs* , 1191–1224 (2020).

[5] Agency, C. S., "Quantum Encryption and Science Satellite (QEYSSat)." https://www.asc-csa.gc.ca/eng/satellites/qeyssat.asp (2023). Accessed: 2015-01-08.

[6] Mazzarella, L., Lowe, C., Lowndes, D., Joshi, S. K., Greenland, S., McNeil, D., Mercury, C., Macdonald, M., Rarity, J., and Oi, D. K. L., "QUARC: Quantum research cubesat—a constellation for quantum communication," *Cryptography* **4**(1), 7 (2020).

[7] Polnik, M., Mazzarella, L., Di Carlo, M., Oi, D. K., Riccardi, A., and Arulselvan, A., "Scheduling of space to ground quantum key distribution," *EPJ Quantum Technology* **7**, 1–34 (2020).

[8] Islam, T., Sidhu, J. S., Higgins, B. L., Brougham, T., Vergoossen, T., Oi, D. K., Jennewein, T., and Ling, A., "Finite-resource performance of small-satellite-based quantum-key-distribution missions," *PRX Quantum* **5**(3), 030101 (2024).

[9] Sidhu, J. S., Brougham, T., McArthur, D., Pousa, R. G., and Oi, D. K. L., "Finite key effects in satellite quantum key distribution," *npj Quant. Inf.* **8**(1), 18 (2022).

[10] Sidhu, J. S., Brougham, T., McArthur, D., Pousa, R. G., and Oi, D. K. L., "Finite key performance of satellite quantum key distribution under practical constraints," *Commun. Phys.* **6**, 210 (2023).

[11] Huang, D., Zhao, Y., Yang, T., Rahman, S., Yu, X., He, X., and Zhang, J., "Quantum key distribution over double-layer quantum satellite networks," *IEEE Access* **8**, 16087–16098 (2020).

[12] Orsucci, D., Kleinpaß, P., Meister, J., De Marco, I., Häusler, S., Strang, T., Walenta, N., and Moll, F., "Assessment of practical satellite quantum key distribution architectures for current and near-future missions," *arXiv preprint arXiv:2404.05668* (2024).

[13] Yu, H.-C., Tang, B.-Y., Chen, H., Xue, Y., Tang, J., Yu, W.-R., Liu, B., and Shi, L., "Airborne quantum key distribution with boundary layer effects," *EPJ Quantum Technology* **8**(1), 1–13 (2021).
[14] Yu, H., Tang, B., Tang, J., Li, J., Cao, Y., Liang, Z., Liu, Y., Sun, Y., Liu, B., and Shi, L., "Quantum key distribution performance analysis under different condition of boundary layer," in [*Thirteenth International Conference on Information Optics and Photonics (CIOP 2022)*], **12478**, 109–118, SPIE (2022).
[15] Yu, H., Tang, B., Li, J., Cao, Y., Zhou, H., Li, S., Xiong, H., Liu, B., and Shi, L., "Satellite-to-aircraft quantum key distribution performance estimation with boundary layer effects," *Chin. Opt. Lett.* **21**, 042702 (Apr 2023).
[16] Berk, A., Conforti, P., Kennett, R., Perkins, T. C., Hawes, F., and van den Bosch, J. M., "MODTRAN6: a major upgrade of the MODTRAN radiative transfer code," in [*Defense + Security Symposium*], (2014).
[17] Lerner, R., "The vuv as a wavelength region for optical intersatellite communications," in [*5th Communications Satellite Systems Conference*], 499 (1974).
[18] Abasifard, M., Cholsuk, C., Pousa, R. G., Kumar, A., Zand, A., Riel, T., Oi, D. K., and Vogl, T., "The ideal wavelength for daylight free-space quantum key distribution," *APL Quantum* **1**(1) (2024).
[19] Sidhu, J. S., Brougham, T., McArthur, D., Pousa, R. G., and Oi, D. K. L., "Satellite Quantum Modelling & Analysis Software Version 1.1: Documentation," *arXiv e-prints* , 2109.01686 (2021).
[20] Lu, C.-Y., Cao, Y., Peng, C.-Z., and Pan, J.-W., "Micius quantum experiments in space," *Rev. Mod. Phys.* **94**, 035001 (Jul 2022).
[21] Ursin, R., Jennewein, T., Kofler, J., Perdigues, J. M., Cacciapuoti, L., de Matos, C. J., Aspelmeyer, M., Valencia, A., Scheidl, T., Acin, A., et al., "Space-QUEST, experiments with quantum entanglement in space," *Europhysics News* **40**(3), 26–29 (2009).
[22] Khatri, S., Brady, A. J., Desporte, R. A., Bart, M. P., and Dowling, J. P., "Spooky action at a global distance: analysis of space-based entanglement distribution for the quantum internet," *npj Quantum Information* **7**(1), 4 (2021).
[23] Panigrahy, N. K., Dhara, P., Towsley, D., Guha, S., and Tassiulas, L., "Optimal entanglement distribution using satellite based quantum networks," in [*IEEE INFOCOM 2022-IEEE Conference on Computer Communications Workshops (INFOCOM WKSHPS)*], 1–6, IEEE (2022).
[24] Leone, H., Srikara, S., Rohde, P. P., and Devitt, S., "Upper bounds for the clock speeds of fault-tolerant distributed quantum computation using satellites to supply entangled photon pairs," *Physical Review Research* **5**(4), 043302 (2023).
[25] Gündoğan, M., Sidhu, J. S., Henderson, V., Mazzarella, L., Wolters, J., Oi, D. K., and Krutzik, M., "Proposal for space-borne quantum memories for global quantum networking," *npj Quantum Information* **7**, 128 (2021).
[26] Boone, K., Bourgoin, J.-P., Meyer-Scott, E., Heshami, K., Jennewein, T., and Simon, C., "Entanglement over global distances via quantum repeaters with satellite links," *Phys. Rev. A* **91**, 052325 (May 2015).
[27] Liorni, C., Kampermann, H., and Bruß, D., "Quantum repeaters in space," *New J. Phys.* **23**, 053021 (May 2021).
[28] Gündoğan, M., Jennewein, T., Asadi, F. K., Ros, E. D., Sağlamyürek, E., Oblak, D., Vogl, T., Rieländer, D., Sidhu, J., Grandi, S., Mazzarella, L., Wallnöfer, J., Ledingham, P., LeBlanc, L., Mazzera, M., Mohageg, M., Wolters, J., Ling, A., Atatüre, M., de Riedmatten, H., Oi, D., Simon, C., and Krutzik, M., "Topical white paper: A case for quantum memories in space," (2021).
[29] Wallnöfer, J., Hahn, F., Gündoğan, M., Sidhu, J. S., Wiesner, F., Walk, N., Eisert, J., and Wolters, J., "Simulating quantum repeater strategies for multiple satellites," *Communications Physics* **5**, 169 (Jun 2022).
[30] Wittig, S. E., Wittig, S. M., Berquanda, A., Zhong, M., and Sellars, M. J., "Concept for single-satellite global quantum key distribution using a solid state quantum memory." http://iafastro.directory/iac/paper/id/36863/summary/ (Sep 2017). IAC-17,B2,7,1,x36863.
[31] Gündoğan, M., Sidhu, J. S., Krutzik, M., and Oi, D. K. L., "Time-delayed single satellite quantum repeater node for global quantum communications," *Optica Quantum* **2**, 140–147 (Jun 2024).
[32] Lei, Y., Kimiaee Asadi, F., Zhong, T., Kuzmich, A., Simon, C., and Hosseini, M., "Quantum optical memory for entanglement distribution," *Optica* **10**(11), 1511–1528 (2023).
[33] Drmota, P., Main, D., Nadlinger, D., Nichol, B., Weber, M., Ainley, E., Agrawal, A., Srinivas, R., Araneda, G., Ballance, C., et al., "Robust quantum memory in a trapped-ion quantum network node," *Physical Review Letters* **130**(9), 090803 (2023).
[34] Gao, S., Blackmore, J. A., Hughes, W. J., Doherty, T. H., and Goodwin, J. F., "Optimization of scalable ion-cavity interfaces for quantum photonic networks," *Physical Review Applied* **19**(1), 014033 (2023).